Experimental Analysis of Convective Heat Transfer for Solar Panels in Outdoor Conditions

Liliane Bou Nassif, Stéphanie Giroux-Julien, Hervé Pabiou

Experimental Analysis of Convective Heat Transfer for Solar Panels in Outdoor Conditions

Liliane Bou Nassif[1]✉, Stéphanie Giroux-Julien[2], and Hervé Pabiou[1]

[1] Univ Lyon, INSA-Lyon, CNRS, CETHIL UMR5008, F-69621 Villeurbanne, France,
liliane.bou-nassif@insa-lyon.fr
[2] Univ Lyon, Université Claude Bernard Lyon 1, CNRS, CETHIL UMR5008,
F-69622 Villeurbanne, France

Abstract. This paper addresses the challenges associated with predicting the temperature of solar cells under operating conditions, which is crucial for optimizing performance and reducing the risk of system failure for PV system designers and operators. The conventional approach of estimating solar cell temperature using thermal models based on energy balance presents significant uncertainties, particularly with the convective heat transfer coefficient, which is difficult to measure and depends on various parameters. To overcome these challenges, this paper focuses on the measurement protocol for the convective heat transfer coefficient and the identification of the main influencing parameters. As reported in the literature, the results show a linear variation with the wind velocity within a relatively narrow domain of validity. The influence of two main parameters is investigated: the location of the sensor and the orientation of the panels with respect to the direction of the dominant wind. It should be noted that all the obtained results will be valid mainly for this particular analyzed situation: The bi-slope power plant configuration with panels installed in an east-west dual-sided format and a 12° tilt.

Keywords: Solar Energy, Convective Heat Transfer Coefficient, Measurement, Urban Environment

1 Introduction

Technology based on mono or poly-crystalline silicon represents 95% of the global market for photovoltaic (PV) components [1]. However, this technology has a temperature-dependent efficiency that decreases power as the temperature of the solar cell increases [2, 3]. For example, under extreme conditions, the temperature of the solar panel can reach 70°C [4], resulting in a 4-point drop in efficiency with respect to standard test conditions. Therefore, predicting solar cell temperature in operating conditions is essential for PV system designers and operators to optimize performance and reduce the risks of system failure. Nevertheless, the

estimation of solar cell temperature can be challenging as it depends on many factors, including the ambient temperature, the solar irradiance, and the wind speed. A common method of estimating solar cell temperature is to use thermal models based on energy balance, where heat transfer from the panel to the environment is modeled by a total heat transfer coefficient (HTC) which is the sum of a radiative part and a convective part [5], the former being a major source of uncertainty in the prediction production. Two main reasons may explain the uncertainty: 1) The convective HTC is very difficult to measure, especially under sunshine 2) The construction of suitable models to feed the computer codes is made difficult by the fact that the convective HTC depends on many parameters. Concerning measurement methods, some authors use fluxmeters for high-flux applications [6] and for building applications [7, 8]. In the former case, authors are mainly interested in the total heat transfer and notice that the determination of the convective heat transfer coefficient is the major source of uncertainty. For the design and optimization of PV systems, the convective HTC is derived from empirical laws. The correlations classically used in the literature [9, 10], link the convective exchange coefficient only to the mean wind speed by a linear or power law relation. Hence, it is reasonable to think that other factors should be taken into account, such as wind direction or velocity fluctuations in the neighborhood of the surface. On the other hand, there is a very large dispersion of a factor of 10 in the values predicted by the different laws [11], this very large dispersion justifies the need for in-depth work on the metrology of the convective exchange coefficient.
In this study, the first objective is to give an experimental protocol to measure the convective HTC in outdoor conditions, and the second is to determine influencing parameters in outdoor conditions.

2 Experimental Setup

2.1 Platform Presentation

The solar platform of CETHIL is a $33m^2$ area on the roof of a building on the Campus Lyon Tech la Doua in Lyon, France. It is dedicated to the analysis of solar components in outdoor conditions. For this study, 12 PV modules are installed on the platform in a bi-slope power plant configuration. The panels are installed in an east-west dual-sided format with a tilt of 12° (Fig.1).

The campaign focuses on the thermal and electrical monitoring of a module in the center of the group. It operates at the maximum power point thanks to a programmable electronic load using the incremental conductance method. Thermal monitoring is carried out by direct temperature measurement using 120μm diameter K-type thermocouples glued to the back of the panel at multiple points. All thermocouples are calibrated using a calibration well (Fluke 9142), resulting in an uncertainty of $\pm 0.1K$. A single heat flux sensor (Captec) is used to locally measure the total heat flux at the center of the front surface of the module. It is painted black, and the emissivity is measured in the short wave range [0.27–1.1]μm at the Lyon Institute of Nanotechnology and in the long wave

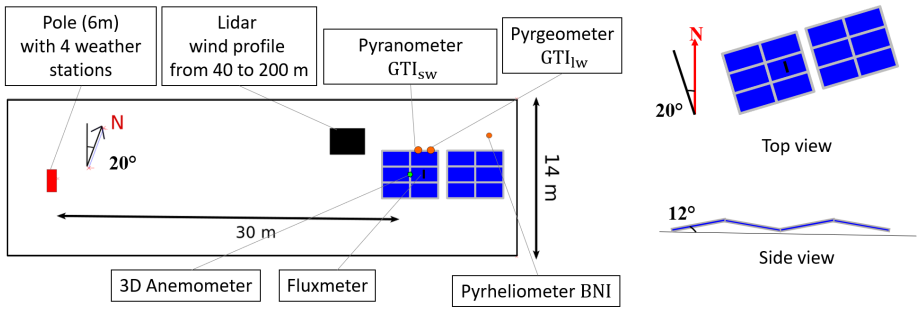

Fig. 1. On the right: top view of the experimental setup on the roof of the building at 16m above the ground. On the left: top and side views of 12 solar panels oriented in an east-west direction with an inclination angle of 12 degrees. N indicates the north direction.

range $[2.5-20]\mu m$ at CETHIL. The shape of the sensor is custom-made to avoid shading effects. Regarding the monitoring of weather data, the solar platform is equipped with a pyranometer Kipp-Zonen CMP22 and a pyrgeometer Kipp-Zonen CGR4, both installed in the same plane as the Captec fluxmeter. This plane is oriented 12 degrees from the horizontal plane (Fig.1). These instruments are used to measure the global tilted irradiation in the short wave (GTI_{sw}) and long wave (GTI_{lw}), respectively. All these sensors are connected to a digital multimeter (Keithley 3706), and the data is collected at a sampling rate of 1Hz. Wind is measured by four weather stations located at an altitude of 2m, 3.25m, 4.75m, and 6m above the roof on a mast located 30m from the solar platform (Fig.1). Two components of the wind speed and temperature are averaged over 10 minutes and collected at a sampling rate of 1Hz. A 3D sonic anemometer is located very close to the solar panel (<1m from the heat fluxmeter). It records the instantaneous values of the three velocity components at a sampling rate of 1Hz. A Lidar Wind Profiler installed near the solar platform records the wind speed profiles from 40 to 200 meters above the roof, along with the direction of the wind relative to the south direction. The data is sampled at a rate of 1 Hz.

All data are preprocessed to obtain a homogeneous set of data. The data is initially averaged over a one minute interval, which corresponds to a one-minute frequency. Subsequently, a 10 minute rolling average is applied, resulting in a sampling frequency of 1/60 Hz. In this study, the data collection was conducted on 24 specific days selected from the period August 2022 to June 2023, each consisting of a 10-hour period. This time frame was deliberately selected to align with the sunniest and warmest days, providing an optimal environmental setting for assessing the measurement methodology.

2.2 Measurement Protocol for Convective HTC

The local HTC is measured at the module's center for precision, but to apply it to the entire PV system's thermal model, certain assumptions are required. The

total heat flux measured by the sensor (q_{fluxm}) on the front surface is the sum of a radiative part (q_{rad})and a convective part (q_{conv}) (Eq.(1))

$$q_{fluxm} = q_{rad} + q_{conv} \tag{1}$$

The convective HTC (h_{conv}) is defined by Eq.(2):

$$q_{conv} = h_{conv}(T_{fluxm} - T_{air}) \tag{2}$$

where T_{fluxm} is the temperature of the sensor and T_{air} is the temperature of the air measured in the vicinity of the sensor, below the panel, protected from the sun, and outside the boundary layer. To estimate the radiative part of the total heat flux, we assume that the surface of the sensor is diffuse and grey over the short wave range and the long wave range. Under these assumptions, the net radiative heat flux is calculated by Eq.(3):

$$q_{rad} = \varepsilon\sigma T_{fluxm}^4 - (\alpha_{sw} GTI_{sw} + \alpha_{lw} GTI_{lw}) \tag{3}$$

where $\sigma = 5.67.10^{-8}\mathrm{W.m^{-2}.K^{-4}}$ is the constant of Stephan-Boltzmann, $\varepsilon = 0.95$ is the total emissivity of the heat fluxmeter, ($\alpha_{sw} = 0.94, \alpha_{lw} = 0.93$) are the absorptivity in the short and long wave ranges, respectively. Therefore, q_{rad} is estimated from measurements, and it is subtracted from the total heat flux to obtain the convective heat flux and finally the convective HTC.

The averaged absorptivity and emissivity of the fluxmeter are radiative parameters that rely on the black coating applied and are assessed by two spectrometric protocols. The spectral measurements encompass the visible range of 280 nm to 1100 nm, as well as the infrared spectrum spanning 2000 nm to 20000 nm. However, the pyranometer and pyrgeometer measure the electromagnetic field between boundaries that differ from the ones used in the spectral measurements. The short-wave band for the pyranometer sensor ranges from 285 nm to 2800 nm, while the long-wave band for the pyrgeometer sensor covers 4500 nm to 42000 nm. The absorptivity and emissivity of the coating are both determined via a weighted integral, assuming that spectral measurements remain constant in the spectral range outside the measurement range. The hemispherical power of the heat flux sensor can be described as shown in Eq.(4):

$$\varepsilon(T_{fluxm}) E_b(T_{fluxm}) = \int_0^\infty \varepsilon_\lambda(T_{fluxm}).E_{\lambda,b}(T_{fluxm})\, d\lambda \tag{4}$$

whith ε_λ, $E_{\lambda,b}$ and E_b being the spectral emissivity, the blackbody spectral emission, and the total emissive power, respectively.

2.3 Instrumented Plate for Validation

An instrumented plate is designed to assess the measurement of the convective HTC. It consists of a 200 × 1900mm instrumented plate made up of a 50mm-thick insulating board covered with 50μm black aluminum tape (Fig.2). A heat

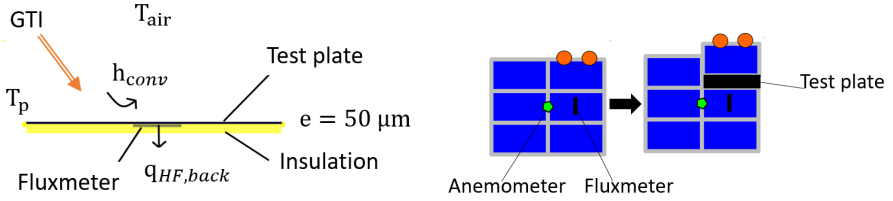

Fig. 2. Experimental device to validate the measurement of the convective HTC. Left: measuring principle; right: location of the instrumented plate in the setup.

fluxmeter is positioned on the back side of the plate to measure the heat rate through the insulating board ($q_{HF,back}$). A thermocouple is put between the heat fluxmeter and the aluminum tape. The test plate is positioned between two PV modules. The convective HTCs on the instrumented plate and on the solar panel are supposed to be equal.

For the system depicted in Fig.2, the temperature of the aluminum tape is supposed to be homogeneous, and the energy equation is written in Eq.(5):

$$\rho e C_p \frac{dT_p}{dt} = -h_{conv}(T_p - T_{air}) - \varepsilon\sigma T_p^4 + \alpha_{lw} GTI_{lw} + \alpha_{sw} GTI_{sw} - q_{HF,back} \quad (5)$$

where ρ, e, C_p, T_p are the density, thickness, thermal capacity, and temperature of the aluminum tape, respectively. Therefore, the coefficient h_{conv} can be obtained from the measurements at each time.

3 Results

3.1 Measurement Data Correction Techniques

The validity of the measurement methodology is assessed by comparing the value of the convective HTC given by the fluxmeter method with the reference value given by the instrumented plate, as shown in Fig.3. The validation is made by using a sample recorded over a 3-day period. Raw values of the convective HTC ($h_{conv,raw}$) are found to be unexpectedly large. A visual inspection of the sensor clearly shows the deterioration of the fluxmeter's paint and the accumulation of dust. Therefore, the error in the HTC is attributed to the value of the absorptivity in the shortwave range. Let $\delta\alpha_{sw}$ be the gap between the real value of the absorptivity ($\alpha_{sw,True}$) and the value measured on the fresh-painted sensor (α_{sw}):

$$\alpha_{sw} = \alpha_{sw,True} + \delta\alpha_{sw} \quad (6)$$

This error leads to a variation in the net radiative heat flux:

$$q_{rad} = q_{rad,True} + \frac{\partial q_{\mathrm{rad}}}{\partial \alpha_{\mathrm{sw}}} \delta\alpha_{sw} \quad (7)$$

$$= q_{rad,True} - GTI_{sw}\delta\alpha_{sw} \quad (8)$$

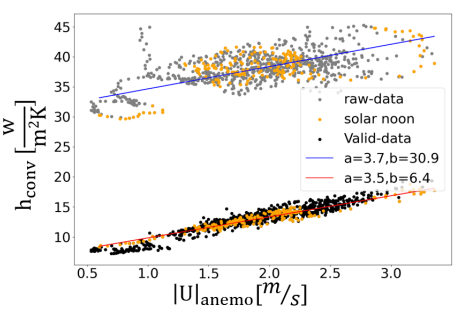

Fig. 3. Convective HTC measured by both the heat fluxmeter and the instrumented plate method against wind speed measured by the 3D anemometer (whole set in gray, selected set in orange at solar noon).

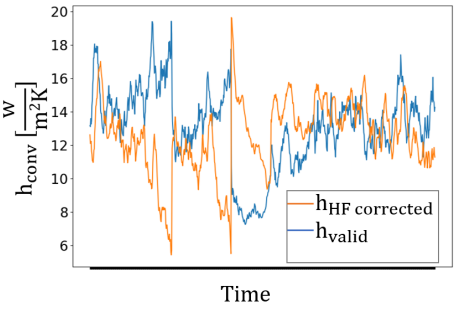

Fig. 4. The temporal evolution of the convective coefficient, measured and corrected using the flux metric method, as well as the coefficient measured by the instrumented plate depicted for a 3-day data set.

where Eq.(3) has been used. Then, considering Eqs.(1), (2), Eq.(7) can be written:

$$h_{conv,raw} = \frac{q_{fluxm} - q_{rad,True}}{T_{fm} - T_{air}} + \frac{GTI_{sw}\delta\alpha_{sw}}{T_{fm} - T_{air}} \tag{9}$$

So, one obtains the corrected value of the convective HTC ($h_{conv,corr}$):

$$h_{conv,corr} = h_{conv,raw} - \frac{GTI_{sw}\delta\alpha_{sw}}{T_{fm} - T_{air}} \tag{10}$$

The values of the convective HTC values shown in Fig.3 are computed with different values of absorptivity to match the measurements obtained by the instrumented plate. A error $\delta\alpha_{sw}$ of 0.45 is obtained. Therefore, the raw value of the convective coefficient measured by the fluxmetric method can be corrected by adjusting the value of the absorptivity α_{sw} from 0.94 to 0.49. Fig.4 displays the corrected value of the convective coefficient measured by the heat fluxmeter method $h_{conv,corr}$ alongside the reference value measured by the instrumented plate, denoted as h_{valid}. In the rest of the article, the value of the convective HTC is corrected by this method and it is denoted h_{conv}.

3.2 Dataset Presentation

The analysis of the evolution of the convective HTC is based on data collected on 24 specific days of 10 hours selected from the period August 2022 to June 2023, providing a favorable environmental context to evaluate the measurement methodology. The acquisition loop is configured to record data every minute. A total of 11650 valid data points were collected during this period (≈1 data/min x 10h/period). All measurements are filtered with a Gaussian low-pass filter with a typical time of 10 min.

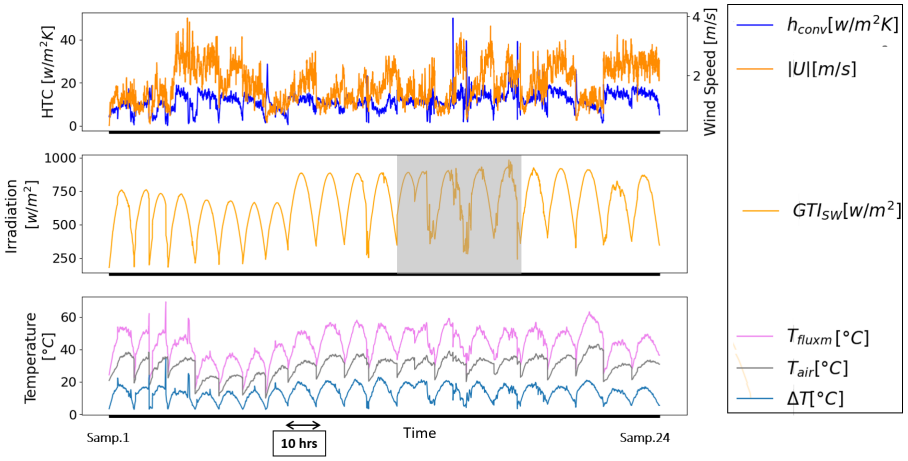

Fig. 5. Temporal evolution of the data set where $\Delta T = T_{fluxm} - T_{air}$. The gray band indicates partly cloudy days.

Fig.5 illustrates the temporal evolution of meteorological parameters: the magnitude of the wind speed measured by the anemometer $|U|$, global tilted shortwave irradiation measured by the pyranometer, air temperature, fluxmeter temperature, and the convective HTC.

To establish a classical correlation, the convective HTC is plotted against wind intensity measured by the 3D sonic anemometer in Fig.6, with gray dots representing the entire sample. Analysis of the data reveals that the dispersion can be significantly reduced when the data set is limited around solar noon, which is defined in this study by the following criterion: $GTI_{sw} \geq 0.95 \max(GTI_{sw})$. As expected, the dispersion is reduced, and the data can be reasonably fitted by a linear equation with a root mean square error (RMSE) of 7% which is quite good accuracy for such correlations. Therefore, it is important to notice that such linear correlations, largely used in the literature, have a narrow scope of validity. Fig. 6 displays variations in HTCs, influenced by wind speed measurements and calculations [11]. Our study aligns with Mc Adams but not with others, high-

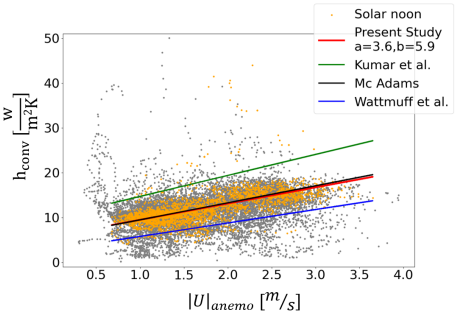

Fig. 6. Convective HTC against wind speed measured by the 3D anemometer (whole set in gray, selected set in orange at solar noon) a and b are the coefficients of the linear law. $h_{conv} = a|U| + b$.

lighting the need to refine these correlations and understand the source of these variations. This underlines the importance of further research into meteorological factors affecting heat exchange.

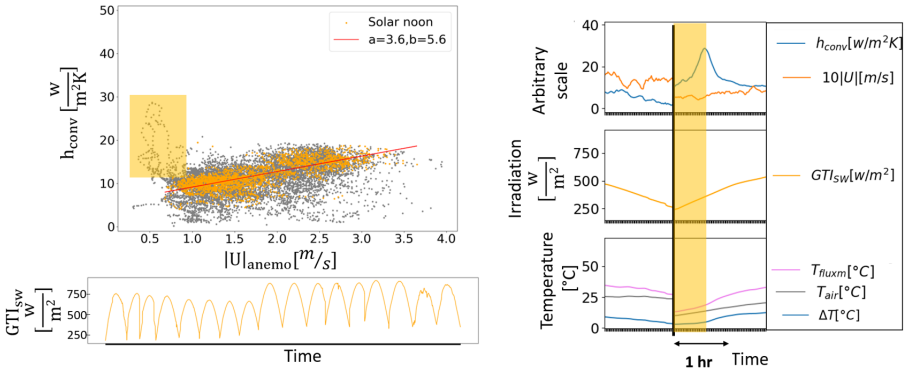

Fig. 7. On the right: convective HTC plotted against wind speed, measured by the 3D anemometer. The entire data set is represented in gray, while the selected subset during solar noon is highlighted in orange after excluding partly cloudy days. On the left: the temporal progression of data set sample 8, unveiling outlier points.

In order to analyze the outlier points shown in Fig.6, the data from partly cloudy days (identified by the gray band in Fig.5) are excluded from the dataset. The subset of data is plotted in Fig.7 (left), and one can see that most of the outlier points correspond to cloudy days where the solar radiation is particularly unsteady. However, there are remaining outlier points enclosed within the box in Fig.7. These points are found to be related to an unsteady situation that results in a phase shift between the total heat flux q_{fluxm} and the temperature difference $\Delta T = T_{fluxm} - T_{air}$. An example is shown in Fig.7 (right), where the thermal inertia of the solar panel limits the increase in temperature, whereas the response of the sensor to a change in solar radiation is much faster. Such an inertia effect leads to outlier values of h_{conv} that are not to be considered.

3.3 Influence of Wind Direction and Wind Sensor Position

This study focuses on the influence of wind direction, measured by the 3D anemometer, and the location of the sensor to obtain the wind magnitude.

Fig.8 shows the impact of wind direction. The data set is partitioned into 8 distinct sectors denoted $S_1 - S_8$, each covering a 45-degree span. S_1 corresponds to a wind blowing toward West-South, and sectors are numbered in the clockwise direction. This plot pertains to sectors 3, 4, 5, and 6, focusing on a selected data set during solar noon. Notably, the linear correlation parameters exhibit minimal divergence across these sectors. This outcome is expected as the solar panels are nearly horizontal (the tilt is 12°).

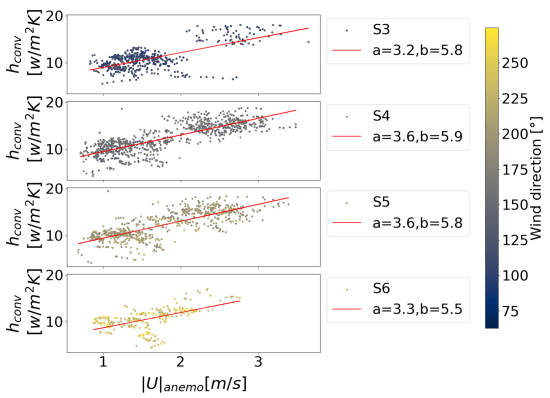

Fig. 8. Influence of wind direction measured by the 3D anemometer.

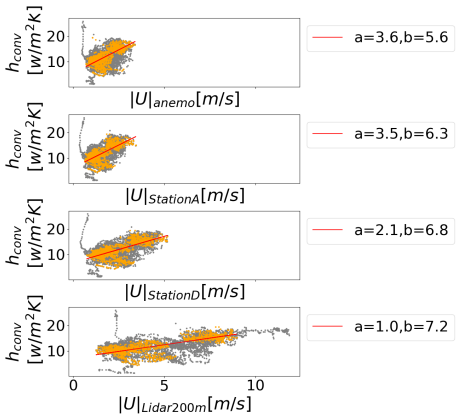

Fig. 9. Influence of wind sensor position on the linear correlation.

To test the influence of the location of the sensor, Fig. 9 shows the results for wind velocities measured by the weather stations (Fig.1) and by the lidar. Station A and D are located 2 m and 6 m above the roof, respectively, and the lidar measures the wind profile at 40 m and 200 m above the roof. The first observation is that, for each case, the HTC can be reasonably approached with a linear fit. The coefficients are quite different, which is expected since the mean velocity increases with altitude. Indeed, Station A, which is approximately at the same altitude as the 3D anemometer, gives almost the same correlation. But for the other sensors, the correlation is different. But in the context of PV power plants, such correlations are used as an input for PV models; hence, it is necessary to rescale the value when the sensor is not at the altitude used to establish the correlation. For example, assuming a neutrally stable atmosphere, the wind profile can be approximated by the classical log-law:

$$U = \frac{u^*}{\kappa} \ln\left(\frac{z - z_0}{h_0}\right) \tag{11}$$

where u^* is the friction velocity, κ is constant of Von-Kármán and the roughness parameters z_0 and h_0 are to be identified for each setup. This identification is part of the perspective of this work: to be able to rescale velocity measured by any sensor.

4 Conclusions and perspectives

Our study presents a methodology for in-situ measurement of the convective HTC under outdoor conditions based on a heat flux sensor. After a calibration to take into account the alteration of the sensor surface, we show that the classical linear fitting of the convective HTC with the magnitude of the wind holds in

a narrow domain of validity. A first analysis of the influence of direction and sensor location is performed. For our nearly horizontal panel (12° tilt), results are almost independent of the direction of the wind. Concerning the position of the sensor, it is found to have a great influence whereas, this parameter is not always given with the correlations used in the models.

Looking ahead, these first results will be improved, and other kinds of correlations will be investigated, such as statistical models.

Acknowledgements

The authors thank Fabien Mandorlo of the Institut des Nanotechnologies de Lyon and Agnès Delmas of CETHIL for spectrometry measurements.

References

1. IEA, Solar PV (2022) https://www.iea.org/reports/solar-pv
2. Tian, H., Mancilla-David, F., Ellis, K., Muljadi, E. Jenkins, P. A.: cell-to-module-to-array detailed model for photovoltaic panels. Solar Energy 86, 2695–2706 (2012).
3. Skoplaki, E. Palyvos, J. A.: On the temperature dependence of photovoltaic module electrical performance: A review of efficiency/power correlations. Solar Energy 83, 614–624 (2009).
4. Kurtz, S. et al.: Evaluation of high-temperature exposure of rack-mounted photovoltaic modules. in 34th IEEE Photovoltaic Specialists Conference (PVSC) 002399–002404 (2009). doi:10.1109/PVSC.2009.5411307
5. Notton, G., Cristofari, C., Mattei, M. Poggi, P.: Modelling of a double-glass photovoltaic module using finite differences. Applied Thermal Eng. 25, 2854–2877 (2005).
6. Vega, T., Wasson, R. A., Lattimer, B. Y. Diller, T. E. Partitioning measurements of convective and radiative heat flux. International Journal of Heat and Mass Transfer 84, 827–838 (2015).
7. Evangelisti, L., Guattari, C., Gori, P., de Lieto Vollaro, R. Asdrubali, F. Experimental investigation of the influence of convective and radiative heat transfers on thermal transmittance measurements. International Communications in Heat and Mass Transfer 78, 214–223 (2016).
8. Evangelisti, L., Guattari, C., Gori, P. Bianchi, F. Heat transfer study of external convective and radiative coefficients for building applications. Energy and Buildings 151, 429–438 (2017).
9. Ghabuzyan, L., Pan, K., Fatahi, A., Kuo, J. Baldus-Jeursen, C.: Thermal effects on photovoltaic array performance: Experimentation, modeling, and simulation. Applied Sciences 11, 1460 (2021).
10. Sharples, S. Charlesworth, P. S.: Full-scale measurements of wind-induced convective heat transfer from a roof-mounted flat plate solar collector. Solar Energy 62, 69–77 (1998).
11. Kumar, S. Mullick, S. C. Wind heat transfer coefficient in solar collectors in outdoor conditions. Solar Energy 84, 956–963 (2010).